Lithium-molybdate nanostructures grown on the Mo(001)surface

Fernando Stavale, Niklas Nilius,* and Hans-Joachim Freund

Fritz-Haber-Institut der Max-Planck-Gesellschaft, Faradayweg 4-6, D-14195 Berlin, Germany

Abstract: Ordered Li–Mo mixed-oxide films of different compositions have been grown on a Mo(001) surface and analyzed by means of scanning tunnelling microscopy, low-energy-electron-diffraction and cathodoluminescence spectroscopy. Starting from a disordered Li_xO ad-layer grown at room temperature, a *scheelite*-type Li_2MoO_4 phase develops on the Mo surface after annealing to 700 K. The building blocks of this structure are regular nanorods of approximately 30 nm length, which exhibit strong light emission in the green spectral range upon electron injection. Further annealing induces a restructuring of the film that evolves into various mixed-oxide phases of decreasing Li content. The Li fully desorbs from the surface above 1000 K, leaving behind a nano-crystalline Mo-oxide. Our approach demonstrates that ternary Li-Mo oxides of high structural quality can be grown as thin films, making them accessible to conventional surface science techniques without charging problems.

Keywords: molybdate; lithium; thin films; scanning tunnelling microscopy; luminescence spectroscopy; heterogeneous catalysis

* nilius@fhi-berlin.mpg.de

1. INTRODUCTION

Ternary and multi-component oxide systems play an important role in heterogeneous catalysis, as they exhibit unique chemical and physical properties that cannot be found in binary oxides.[1,2] The versatility of mixed oxides arises from the interplay of the different cations that fulfil complementary tasks in the compound, such as improving the temperature stability, providing suitable adsorption and reaction sites on the surface and acting as charge donors or acceptors.[3] Moreover, the structure and composition of mixed oxides can be varied over wide ranges, opening efficient pathways to adopt the properties of such materials to the needs of a given application. Molybdates represent a particularly interesting class of materials, as they form the basis for highly reactive and selective catalysts especially for the oxidation of hydrocarbons.[4,5] They also find applications as electrode materials in lithium batteries,[6] as light-emitting phosphors,[7] and corrosion inhibitors.[8] Molybdates in different frameworks turned out to be thermo-dynamically stable and can therefore be used as catalysts in high temperature reactions without deactivation over years.[9] The main factor controlling the performance of molybdates and Mo-oxides in catalysis was shown to be the charge state of the surface species that should be as high as possible to stimulate oxidation processes.[,10] The role of surface defects, on the other hand, has hardly been investigated in such materials so far.[11,12]

One of the technologically most relevant molybdate is Li_2MoO_4 that has been exploited as catalyst for the methane oxidation and finds applications in lithium batteries.[6,13] Li-molybdates were prepared with a variety of methods, including wet-chemical and sol-gel techniques as well as combustion synthesis.[14,15,16] Transmission-electron microscopy, X-ray diffraction and luminescence spectroscopy are the classical tools to analyze the Li-Mo compound, while surface science techniques are rarely applied due to the insulating nature of the material (4.2 eV band gap).[17,18] In this work, we demonstrate that well ordered and morphologically defined Li-molybdates nanostructures can be produced by depositing Li onto Mo(001) followed by different annealing steps in oxygen. Due to their limited thickness, the films are insensitive against charging and can be probed with all common surface science techniques. The ternary Li-Mo oxide grows in the form of uniform nanorods, as seen in scanning-tunnelling-microscopy (STM) images. Information on structural and electronic properties was derived from low-energy-electron-diffraction (LEED) and cathodoluminescence spectroscopy. Owing to their nano-crystalline nature, we expect the Li-Mo-O films to display unique physical and chemical properties that cannot be found in the respective bulk materials.

2. EXPERIMENT

The measurements were performed in an ultrahigh vacuum chamber (2×10^{-10} mbar) equipped with a liquid-nitrogen cooled STM and standard tools for sample preparation and analysis. The STM setup was

designed specifically to detect photons emitted from the tip-sample junction.[19] For this purpose, a Beetle-type head was placed inside a parabolic mirror with the tip being in the focal point. The mirror collects light from a large solid angle of the tunnel junction. A second mirror outside the vacuum focuses the light onto the entrance slit of a grating spectrograph (150 lines/mm) coupled to a liquid-nitrogen cooled charge-coupled-device. The optical setup allows us to detect very low photon fluxes in a wavelength range of 200-1200 nm. All STM images presented here were obtained at LN_2 temperature in the constant current mode using Ag tips. The bias voltage is given with respect to the sample.

The Mo(001) substrate was prepared by cycles of Ar^+ sputtering and annealing to 2000 K, as monitored with an infrared pyrometer. The first cycles were performed in O_2 ambience in order to remove carbon from the surface. The as-prepared sample displayed a sharp (1×1) square pattern in LEED and wide, atomically-flat terraces in STM. Li was deposited from a commercial SAES dispenser onto the Mo substrate at ~350-400 K. The coverage was calibrated via deposition onto MgO thin films, where Li grows into monolayer islands the surface fraction of which is readily determined with STM.[20]

3. RESULTS

An STM topographic image of Mo(001) after 2 ML Li exposure is shown in Fig. 1a. The surface is covered with nm-sized protrusions that exhibit neither an internal structure nor a long-range order. Also the suppression of the (1×1) LEED pattern suggests a disordered Li distribution on the Mo surface. The Li adsorption on metals has been studied in detail before, and a complex c(7√2×√2)R45° super-structure was found for the Mo(001) surface.[21,22,23] The absence of any ordered Li phase in our case might be explained with inappropriate dosing conditions or the presence of residual oxygen/water in our chamber. Depositing the same amount of Li in 5×10^{-7} mbar O_2 leads to a coarsening of the surface and the formation of ad-particles with 3-4 nm diameter and 0.6 nm apparent height (Fig. 1b). Given the high reactivity of Li, we expect those particles to be made of Li_xO. Also this phase is amorphous as no LEED pattern is detected. The morphology of the ad-layer changes completely upon annealing to 700 K in UHV, when a characteristic stripe pattern comprising parallel nanorods of ~2 nm width, ~1 nm height and up to 30 nm length develops on the surface (Fig.1c,d).[24] Already a single stripe seems to be a thermodynamically stable unit, as isolated stripes with similar geometric parameters are found at much lower Li loads (Fig. 1c, inset). The stripes align with the two Mo⟨100⟩ directions and thus develop two orthogonal domains. We suggest that the observed surface reorganization is the result of Li-Mo intermixing at the elevated temperature.

The crystalline nature of the nanorods is deduced from a sharp, yet complex LEED pattern, as shown in Fig. 2. The LEED reflexes can be divided into two groups. Spots of the first group form a simple square pattern and move towards the centre of the LEED screen with increasing electron energy (dashed circles).

They are readily identified as the Mo(001) spots and can be used as internal reference in the diffraction pattern. The second group shows an atypical behaviour, as the spots already appear at very low energies (below 35 eV) and propagate outward with increasing electron energy (Fig. 2, arrows). This behaviour is incompatible with electron diffraction at atomic planes perpendicular to the electron beam, where the increase of the scattering vector with energy always pushes the diffraction spots towards the centre of the LEED screen where they collapse into the (0,0) spot. The occurrence of outward propagating spots thus indicates the presence of facets that are tilted against the macroscopic sample surface.[25] The tilt direction is given by the crystallographic direction along which the spots move in reciprocal space, which are the Mo⟨100⟩ directions in our case. The tilt angle can only be approximated here because the (0,0) spots of the individual facets are already outside the screen. A rough approximation yields a tilt angle $\alpha > 45°$ with respect to the surface plane. We show later that this particular LEED pattern can be reconciled with a facetted Li-molybdate structure growing in two domains on the Mo(001) surface.

Further annealing to 800 K causes the film morphology to change again (Fig. 3a,b). Instead of tall and long nanorods, flat islands that tend to wet the Mo surface are now observed in the STM topographies. The islands are approximately 0.3 nm high and exhibit a line pattern with 1.0-1.2 nm spacing on their top. Occasionally, bundles of two/three protruding lines are disrupted by a chain of dark holes with 0.5-0.6 nm periodicity along the axis (Fig. 3a inset). This is the same periodicity as revealed from the (2×2) LEED pattern observed upon annealing, suggesting that the fundamental building blocks of the new islands structure are 0.63×0.63 nm^2 in size. The island edges are aligned again with the Mo⟨100⟩ directions. When annealing to even higher temperature in UHV (900 K), the flat islands break apart into small rectangular units of 1.2-3.0 nm length and 0.6-1.2 nm width (Fig. 3c,d). Closer inspection reveals that they comprise similar structural elements as the flat islands before, i.e. they are of similar height and consist of rows of 0.5-0.6 nm spacing. In large scale image, the rectangular units form a regular pattern with ~1.5 nm periodicity. Also at this stage, a sharp (2×2) pattern in observed in LEED (Fig. 3c). The last step of our annealing series is reached at 1000 K, when a relatively rough surface develops, densely covered by 1 nm-high pyramids. These nanostructures have a rather uniform size of (3.0±0.5) nm and are regularly arranged along the Mo[100] and [010] directions. Accordingly, a 2D Fourier-Transform of topographic images displays a diffuse, yet obvious square pattern that follows the substrate crystallographic directions. LEED measurements on the respective samples show only the weak (1×1) pattern of Mo(001), in which all spots are connected by lines due to a appreciably surface mosaicity.

Additional information on the Li-Mo-O system is obtained from cathodoluminescence spectroscopy using the STM tip as local electron emitter. The spectra are acquired with 150 eV electron energy and 5 nA current, stabilizing the STM tip at ~100 nm above a pre-selected surface region. Figure 4 shows three cathodoluminescence spectra taken on 2 ML metallic Li/Mo(001) and on 2 ML LiO_x/Mo annealed to 700

and 1000 K, respectively (from bottom to top). The first-spectrum is essentially flat with the exception of a sharp 670 nm-emission peak. This spectral feature was already indentified on other Li-containing compounds and relates to optical transitions in Li atoms that desorb from the surface upon electron impact.[20] The measured photon energy of 1.85 eV (670 nm) corresponds to the most intense optical transition in gas-phase Li^0, that connects the excited Li $1s^2 2p^1$ configuration with the $1s^2 2s^1$ ground state.[26] The 670 nm peak thus provides evidence for the existence of loosely bound Li on the surface. Upon annealing the Li/Mo system in oxygen, the 670 nm-band vanishes because metallic Li transforms into the chemically stable nanorod configuration. Simultaneously, a new emission band with relatively large width (FWHM: 0.7 eV) develops at 500 nm (~2.5 eV) wavelength. Further annealing leads to a gradual decrease of the peak intensity until it completely disappears at ~1000K (Fig. 4, top spectrum). Apparently, the light-emitting phase is stable only in a small temperature window ranging from 700 to 800 K.

4. DISCUSSION

As shown in the previous section, an nano-crystalline oxide phase with distinct structural and optical properties can be prepared by depositing a few ML Li onto the Mo(001) surface and annealing it to 700 K in oxygen (Fig. 1c,d). This phase neither develops when Li metal is annealed in vacuum nor when bare Mo(001) is treated in O_2, indicating that all three elements, Li, Mo and O, are involved in the new compound. Several Li-molybdates have been reported in the literature, the composition of which sensitively depends on the initial Li load and the annealing conditions.[16,23,27] However, only the scheelite group exhibits the characteristic 'green' luminescence at 490–550 nm that has been detected here.[7,17] The building blocks of the scheelite structures are slightly distorted MoO_4^{2-} tetrahedrons that are separated from one another by a second type of cations. The most effective separation is obtained with spacious yet light ions, such as alkali and earth alkali species, which renders Li_2MoO_4 and $CaMoO_4$ particularly interesting for applications. The effective decoupling of the MoO_4^{2-} units in these compounds is responsible for the intense 500 nm-emission, which arises from charge-transfer processes between the O-ligands and the Mo-core.[28] The width of the band is governed by residual coupling between neighbouring units, which opens non-radiative decay channels and shortens the lifetime of the excited state.[29] The similar photon response of typical scheelite structures and our samples now suggests that a Li_2MoO_4-type of film develops on the Mo(001) surface upon annealing a Li_xO adlayer to 700-800 K. To support this scenario, we have tried to reconcile not only the optical data but also the LEED and STM signatures of our films with the known properties of Li_2MoO_4.

In a first step, we have considered several crystallographic planes of Li_2MoO_4 to identify a suitable interface with the Mo(001). The bulk phase is made of corner-sharing MoO_4 and LiO_4 tetrahedrons, in

which each MoO_4 unit has eight LiO_4 neighbours connected *via* trigonally-coordinated oxygen ions.[27,30] The most probable cleavage plane is a particular (110) plane that exhibits a minimum of interconnections between the upper and lower half-space. To create the potential interface, the bonds between nine O ions and 6 Mo / 3 Li ions need to be broken per Li_2MoO_4 unit cell. The resulting plane is O-terminated and might therefore readily interact with the Mo(001) support. Using the bulk lattice parameters, even an epitaxial relationship can be achieved between the Li_2MoO_4(110) and Mo(001) plane in the following way (Fig. 5a). The terminating O ions are arranged in double rows of 3.48 Å spacing, separated from the next double row by 5.34 Å. The sum of both values matches three Mo-Mo distances along the Mo[100] with only 5% misfit. Given the high flexibility of nanostructures, row matching seems thus to be feasible with the Mo[100] lying parallel to the Li_2MoO_4[1-10]. However even an atomic register along the rows is likely, as the O-O distance along the [001] direction of the molybdate alternates between two times 3.37 Å (across two Mo tetrahedrons) and one times 2.92 Å (across a Li tetrahedron). The sum matches again three times the Mo-Mo separation along the [010] direction with 2% mismatch only. Consequently, the terminating O ions of the Li_2MoO_4(110) plane can bind to identical sites in the Mo(001) surface, being probably Mo hollow and bridge sites in order to maximize the oxygen coordination. The fact that the required lattice distortion is not equal along the two crystallographic directions also explains the observed unidirectional growth of Li_2MoO_4 and the formation of nanorods (Fig. 1c,d). While the growth is highly favourable in the low strain direction, along which the crystals extend over tens of nm, it terminates after 1-2nm in the orthogonal direction due to the larger misfit.

Given the threefold symmetry of Li_2MoO_4 with respect to the c-axis, we further suggest that the side facets of the nanorods are terminated in a similar fashion as the interface plane, resulting in a triangular cross-section (Fig. 5a). The two side facets would then enclose a 60° angle and be inclined by 60° against the surface plane. The presence of such facets is fully compatible with both, LEED and STM results. In LEED, we observe superstructure spots that move outward with increasing energy, suggesting that the (0,0) reflex of the respective facets is not projected onto the LEED screen anymore. For the given geometry of our LEED setup, this implies that the tilt angle has to be larger than 45°, a value that is inline with the 60° predicted by the structure model. The STM images, on the other hand, show a network of nanorods with triangular height profile. The experimental height to diameter ratio has been determined to 0.5 (2 nm width, 1nm height), which compares to 0.8 for an ideal Li_2MoO_4 triangle structure. Two reasons might account for the remaining difference. First, lateral dimensions are always enlarged in STM measurement due to the effect of tip convolution. Second, the Li_2MoO_4 nanorods may adopt trapezoidal shapes, in which the top-most atoms rows are removed in order to avoid under-coordination of the terminating atoms. Both effect would reduce the measured aspect ratio and reconcile experiment and

proposed structure. We note that our model remains tentative, as no structure-sensitive data is available for the Li_2MoO_4 nanorods at this point and the Li-Mo-O phase diagram is comparably rich.[31]

The nanorod pattern disappears after annealing the surface to 800 K in vaccum, most likely because of removal of Li and/or oxygen from the ad-layer. To rationalize the island morphologies emerging in this heating step (Fig. 3a-d), we have considered molybdate phases with a lower Li-to-Mo ratio than in Li_2MoO_4 and a square basal plane to ensure epitaxial relationship with the Mo(001) lattice. Four phases might be compatible with the experimental observations that are for decreasing Li-to-Mo ratio: rocksalt Li_4MoO_5 (basal plane 0.58×0.58 nm^2), rocksalt $Li_4Mo_2O_6$ (Fig. 5b, basal plane 0.59×0.59 nm^2), hexagonal $LiMoO_2$ (basal plane 0.52×0.58 nm) and $LiMo_8O_{10}$ comprising octahedral cluster chains (Fig. 5c, basal plane 0.59×0.59 nm^2).[32,33,34] All four compounds would produce a (2×2) pattern in LEED and enable an epitaxial growth on the Mo(001) support. Moreover, they all consist of Mo ions in octahedral or pyramidal coordination; only that the actual oxidation state decreases from +6 in Li_4MoO_5, +4 in $Li_4Mo_2O_6$, +3 in $LiMoO_2$ to +2.4 in $LiMo_8O_{10}$. A gradual reduction of the Mo species is indeed expected when annealing a ternary oxide in UHV to higher and higher temperatures. Let's finally note that only $LiMoO_2$ shows a tendency for unidirectional growth due to its rectangular unit cell and the large lattice misfit along one growth direction (17%). Although we abstain from assigning the observed morphologies to specific oxide structures due to the lack of atomic-scale data, we want to emphasize a few points:

(i) No well-ordered MoO_3 phase, being the most stable binary oxide, is expected to develop on Mo(001) due to differences in the lattice symmetry. This becomes evident from a Mo-O-Mo bond angle of 104° and the Mo-O bond lengths of 0.23 nm, which compared to a Mo-Mo distance of 0.315 nm in Mo(001). The incorporation of Li may soften these constraints, as Li-O-Li angles are more flexible and the Li-O bond length is shorter (0.2 nm). Li-Mo mixed oxides are therefore better able to cope with the square symmetry of the Mo(001), in line with the experimental data.

(ii) Upon annealing, the Li progressively desorbs from the surface, which removes the balancing units in the molybdate structures. The Mo-rich phases consequently experience an increasing misfit strain, causing the film to break apart into spatially confined islands. This trend can be followed in the temperature evolution of the morphology, in which the maximum structure size decreases from 20 to 3 nm when rising the temperature from 800 to 900 K (Fig. 3). We believe that the Li-poor sections can be detected in the STM as dark dotted lines that cut through the film (Fig. 3a, inset). Along those lines, the mixed islands break apart into small highly strained units.

(iii) Above 1000 K, the Li finally leaves the surface and therewith all compensating elements that have enabled pseudomorpic growth before (Fig. 3e,f). The lattice mismatch experienced by the remaining MoO_x units triggers a massive surface restructuring that results in the formation of square-shaped pyramids of ~3×3 nm^2 size. The strain field around each nanopyramid is responsible for their ordered

arrangement that still mimics the square symmetry of the (001) surface.[35] We note that a similar surface morphology is directly by annealing bare Mo(001) directly in 5×10^{-7} mbar O_2. However, the nano-pyramids produced in this way exhibit a larger size distribution but no long-range order. Apparently, Li residuals in the annealed mixed films promote the development of less-strained MoO_x–Mo interface structures and improve the overall quality of the oxide film. As the stoichiometriy of the nanopyramids is unknown, we can only speculate on their possible MoO_3 nature. Note that all Li-Mo-O compounds discussed in the latter paragraph are optically inactive, because either the charge-transfer transitions in the $[MoO_4]^{2-}$ tetrahedrons are dipole forbidden or the luminescent units are strongly coupled to an optically inactive environment.[36]

5. CONCLUSIONS

Oxygen-assisted Li deposition on Mo(001) gives rise to the formation of several Li-Mo mixed-oxides with distinct structural and optical properties. At relatively low preparation temperature, a regular stripe pattern develops on the surface that comprises scheelite-type nanorods and exhibits intense light emission in the green spectral range. The loss of Li upon annealing produces a variety of molybdate structures that are characterized by a decreasing Li-to-Mo ratio and lower Mo oxidation states. At 1000 K annealing temperature, all Li is removed and a partly-ordered MoO_x phase develops on the surface. The formation of the various mixed oxides is driven by intermixing of adsorbed Li and Mo atoms from the support, a process that gets promoted by the small ion radius and the low diffusion barriers of Li. As inter-diffusion is limited to a confined region at the Li-Mo interface, our preparation procedure is well suited to produce thin molybdate films but cannot be used to prepare bulk-like samples. Still, the relatively uniform ad-layers presented here may serve as model systems to investigate the adsorption and reaction behaviour of Li-molybdates.

ACKNOWLEDGMENT: F. S. thanks the ‘Alexander v. Humboldt Stiftung’ for financial support. The authors acknowledge support from the DFG through the Cluster of Excellence ‘UniCat’.

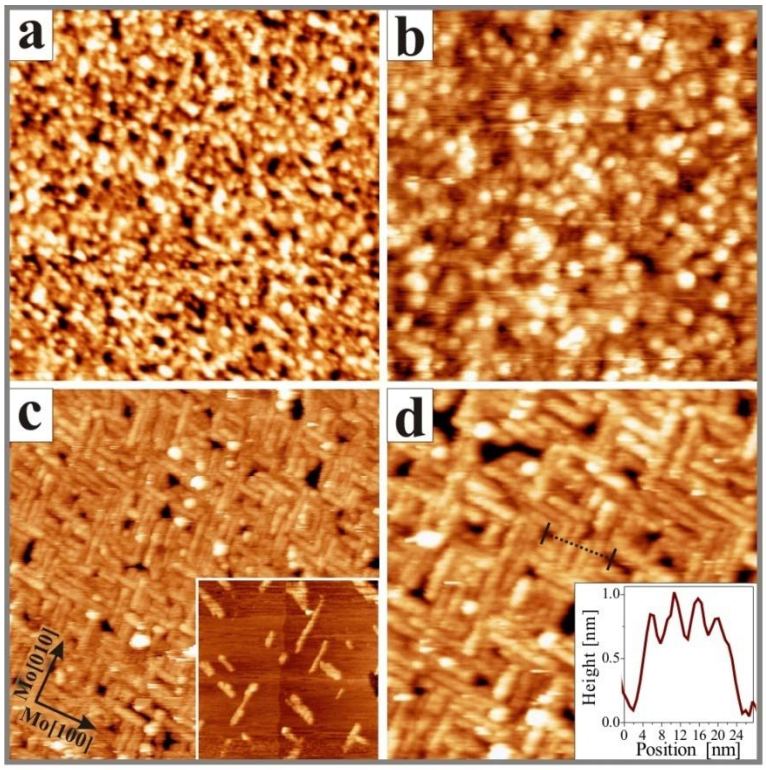

Figure 1: STM topographic images of the Mo(001) surface after depositing **(a)** 2 ML metallic Li and **(b)** 2 ML Li in 5×10^{-7} mbar O_2 (3.5 V, 200×200 nm^2). **(c,d)** Same surface as in (b) but after annealing to 700 K in UHV (4.5 V, 200×200 nm^2 and 100×100 nm^2). The inset in (c) shows the nucleation regime of the Li-molybdate nanorods (1.5 V, 100×100 nm^2). The inset in (d) displays a height profile across the four nanorods marked in the main image.

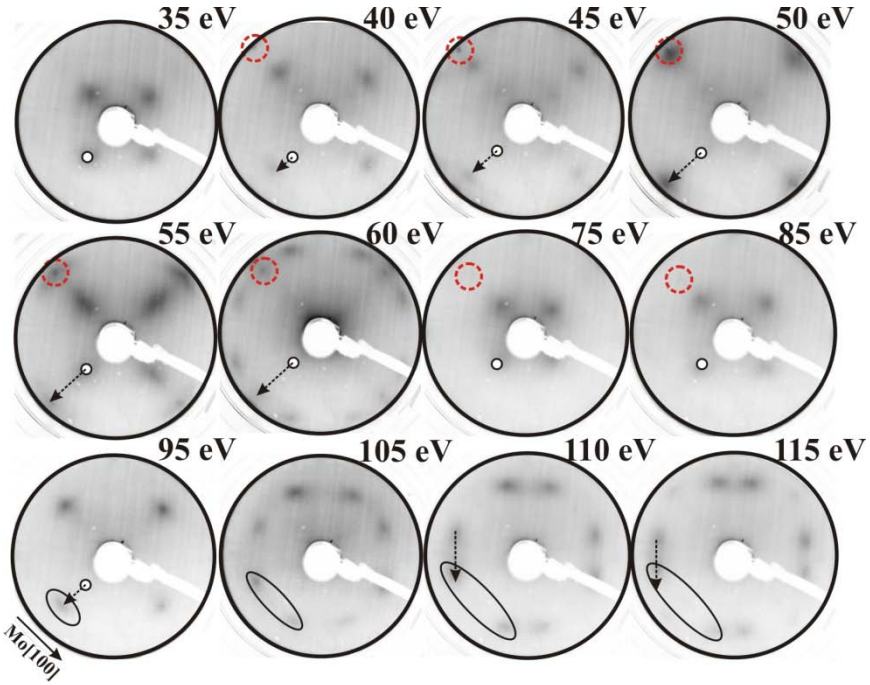

Figure 2: LEED patterns of 2 ML Li-Mo-O annealed to 700 K (scheelite phase). The red, dashed circles mark a Mo(001) spot, whereas the solid ones belongs to the molybdate phase. Movement of the spots with increasing energy are marked by arrows.

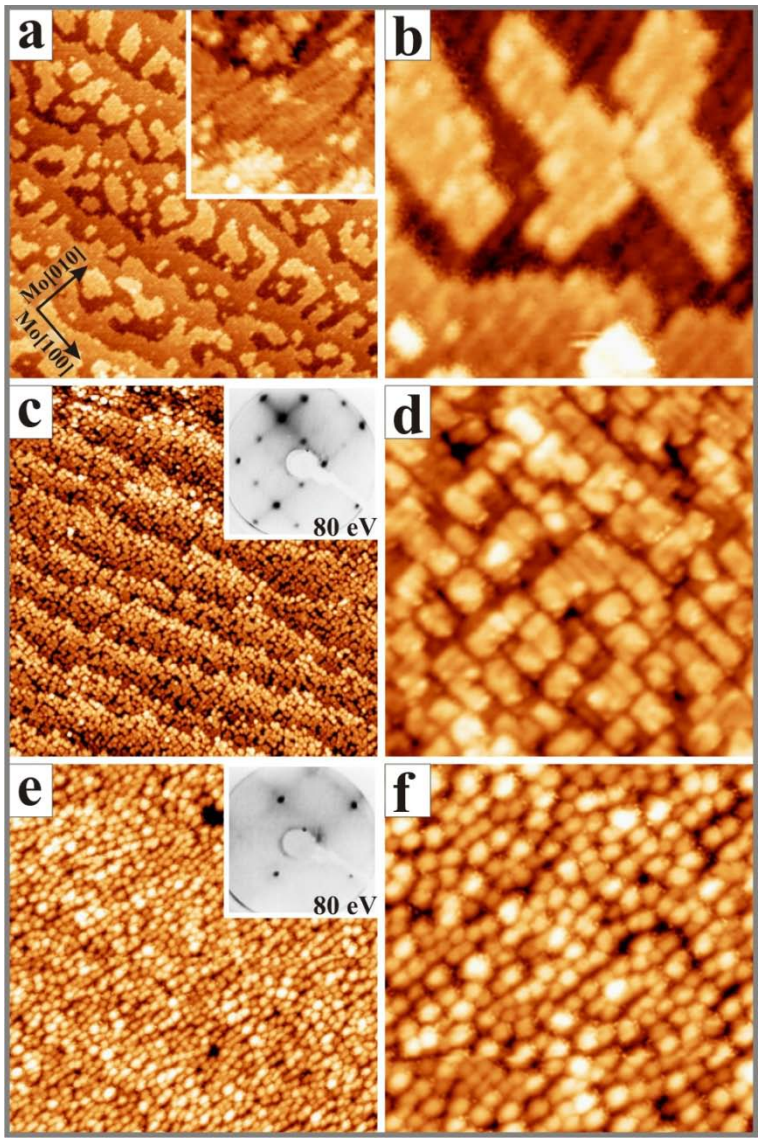

Figure 3: (a,b) STM topographic images of 2ML Li-Mo-O annealed to 800 K (1.6 V, 100×100 nm^2 and 20×20 nm^2). The inset shows a better resolved image that displays the characteristic black dotted lines described in the text (20×20 nm^2). **(c,d)** Same preparation as in (a,b) but annealed to 900 K (1.6 V, 150×150 nm^2 and 20×20 nm^2). The inset shows the corresponding (2×2) LEED. A similar pattern is observed for the samples in (a,b). **(e,f)** Same preparation as in (a,b), but annealed to 1000 K (1.8 V, 150×150 nm^2 and 60×60 nm^2). The inset shows the associated (1×1) LEED. Note the characteristic lines that interconnect the different spots.

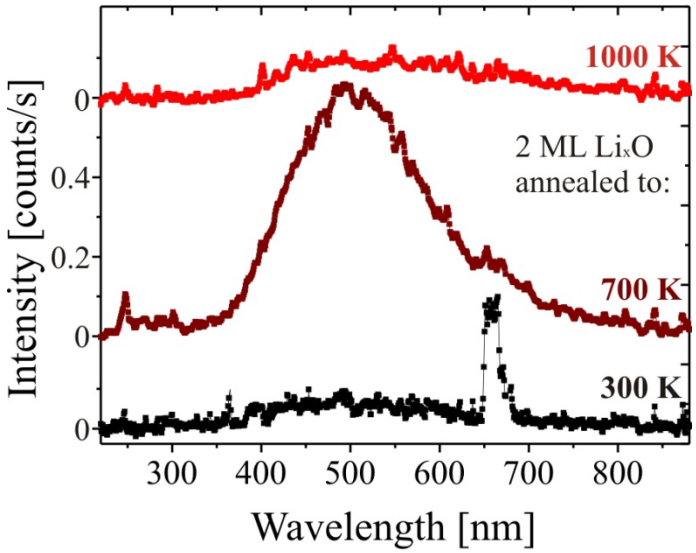

Figure 4: Cathodoluminescence spectra (150 V, 5 nA, accumulation time 300 s) of 2 ML Li/Mo(001) (bottom curve) and of 2 ML Li_xO after annealing to 700 K (central) and 1000 K (upper curve).

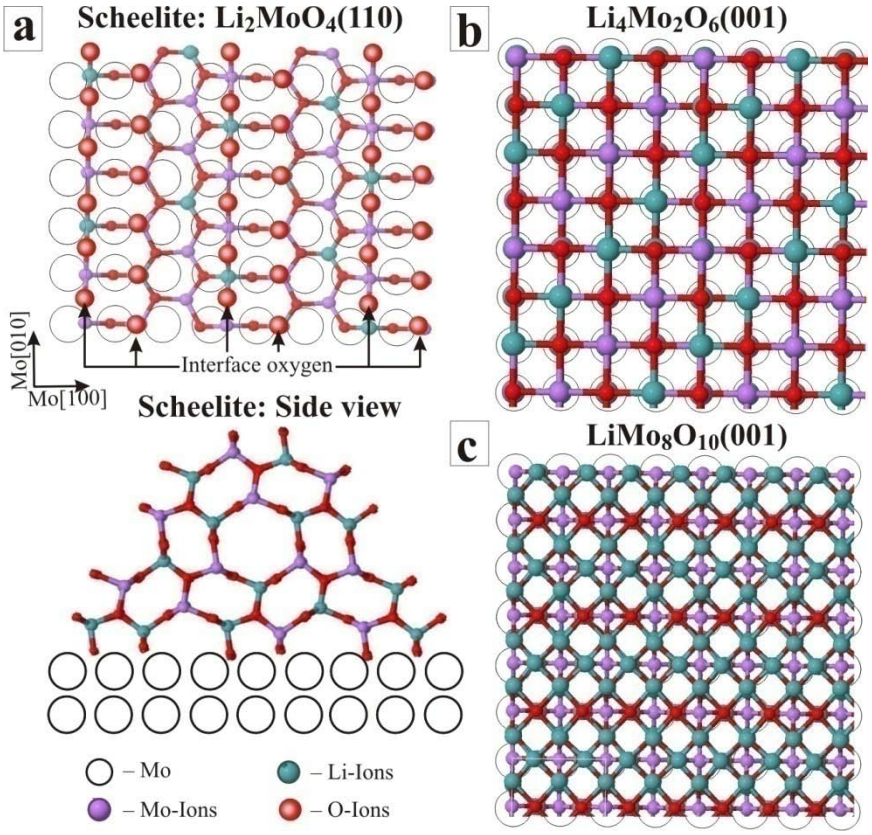

Figure 5: Structure models of potential interfaces between different Li-Mo-O phases and Mo(001): **(a)** Scheelite structure – top and side view, **(b)** $Li_4Mo_2O_6(001)$. Note that the distribution of Li and Mo ions is random in the rocksalt lattice. The Li_4MoO_5 phase has a similar structure only that some of the Mo ions are replaced by Li. **(c)** $LiMo_8O_{10}(001)$**.**

[1] J. B. Torrance, P. Lacorre, C. Asavaroengchai, R. M. Metzger, Physica C 182 (1991) 351-364; L. J. lemany, L. Lietti, N. Ferlazzo, P. Forzatti, G. Busca, E. Giamello, F. Bregani, J. Catal. 155 (1995) 117-130.

[2] G. Ertl, H. Knözinger, F. Schueth, J. Weitkamp, Handbook of heterogeneous catalysis, Weinheim, Wiley-VCH, 2008.

[3] J. D. Perkins, T. R. Paudel, A. Zakutayev, P. F. Ndione, P. A. Parilla, D. L. Young, S. Lany, D. S. Ginley, A. Zunger, N. H. Perry, Y. Tang, M. Grayson, T. O. Mason, J. S. Bettinger, Y. Shi, M. F. Toney, Phys. Rev. B 84 (2011) 205207; M. B. Gawande, R. K. Pandey, R.V. Jayaram, Catal. Sci. Technol. 1 (2012) 1653-1664.

[4] M. M. Bettahar, G. Costentin, L. Savary, J. C. Lavalley, Appl. Catal. A 145 (1996) 1-48.

[5] S. Pradhan, J. K. Bartley, D. Bethell, A. F. Carley, M. Conte, S. Golunski, M. P. House, R. L. Jenkins, R. Lloyd, G. J. Hutchings, Nat. Chem. 4 (2012) 134-139.

[6] L. Sebastian, Y. Piffard, A. K. Shukla, F. Taulelle, J. Gopalakrishnan, J. Mater. Chem. 13 (2003) 1797-1802.

[7] D. Spassky, S. Ivanov, I. Kitaeva, V. Kolobanov, V. Mikhailin, L. Ivleva, I. Voronina, Phys. Stat. Sol. (c) 2 (2005) 65-68.

[8] G. Mu, X. Li, Q. Qu, J. Zhou, Corros. Sci. 48 (2006) 445-459.

[9] A. P. Vieira Soares, M. Farinha Portela, A. Kiennemann, L. Hilaire, Chem. Eng. Sci. 58 (2003) 1315-1322.

[10] Y. A. Saleh-Alhamed, R. R. Hudgins, P. L. Silveston, J. Catal. 161 (1996) 430-440.

[11] J. J. Uhlrich, J. Sainio, Y. Lei, D. Edwards, R. Davies, M. Bowker, S. Shaikhutdinov, H.-J. Freund, Surf. Sci. 605 (2011) 1550-1555.

[12] S. Q. Su, M. M. Biener, C. M. Friend, E. Kaxiras, Surf. Sci. 577 (2005) L71-L77.

[13] A. Erdohelyi, K. Fodor, R. Németh, A. Hancz, A. Oszkó, J. Catal. 199 (2001) 328-337.

[14] Z. Wang, H. Liang, M. Gong, Q. Su, Alloys Comp. 432 (2007) 308-312.

[15] J. Lei, Y. Yu, L. Li, Sh Chneg, G. Li, N. Li, J. Rare Earths 30 (2012) 330-334.

[16] A. C. W. P. James, J. B. Goodenough, J. Sol. Stat. Chem. 76 (1988) 87-96.

[17] R. L. Smith, G. S. Rohrer, J. Solid State Chem. 124 (1996) 104–115.

[18] J. C. Sczancoski, L. S. Cavalcante, N. L. Marana, R. O. da Silva, R. L. Tranquilin, M. R. Joya, P. S. Pizani, J. A. Varela, J. R. Sambrano, M. Siu Li, E. Longo, J. Andrés, Curr. Appl. Phys. 10 (2010) 614-624.

[19] H.-J Freund, N. Nilius, T. Risse, S. Schauermann, T. Schmidt, ChemPhysChem 12 (2011) 79-87.

[20] P. Myrach, N. Nilius, S. V. Levchenko, A. Gonchar, T. Risse, K.-P. Dinse, L. A. Boatner, W. Frandsen, R. Horn, H.-J. Freund, R. Schlögl, M. Scheffler, ChemCatChem 2 (2010) 854-862.

[21] H. P. Bonzel, Surf. Sci. Rep. 8 (1987) 43-125; R. D. Diehl, R. McGrath, Surf. Sci. Rep. 23 (1996) 43-171.

[22] S. H. Payne, H. A. McKay, H. J. Kreuzer M. Gierer, H. Bludau, H. Over, G. Ertl, Phys. Rev. B 54 (1996) 5073-5080, V. Saltas, C.A. Papageorgopoulos, Surf. Sci. 461 (2000) 219-230; J. Kröger, D. Bruchmann, S. Lehwald, H. Ibach, Surf. Sci. 449 (2000) 227-235.

[23] M. L. Hildner, P. J. Estrup, J. Phys. Chem. B 106 (2002) 8456-8465.

[24] I. Ermanoski, K. Pelhos, W. Chen, J. S. Quinton, T. E. Madey, Surf. Sci. 549 (2004) 1-23.

[25] M. Henzler, W. Göpel, Oberflächenphysik des Festkörpers, Teubner, Stuttgart, 1994.

[26] W. Brenig, D.Menzel (Eds.), Desorption Induced by Electronic Transitions: DIET II, Springer, Berlin 1985; M. Wilde, I. Beauport, F. Stuhl, K. Al-Shamery, H.-J. Freund, Phys. Rev. B 59 (1999) 13401-13412.

[27] T. W. S. Yip, E. J. Cussen, C. Wilson, Dalton Trans. 39 (2010) 411-417.

[28] V. M. Longo, A. T. de Figueiredo, A. B. Campos, J. W. M. Espinosa, A. C. Hernandes, C. A. Taft, J. R. Sambrano, J. A. Varela, E. Longo, J. Phys. Chem. A 112 (2008) 8920-8928.

[29] O. P. Barinova, F. A. Danevich, V. Ya. Degoda, S. V. Kirsanova, V. M. Kudovbenko, S. Pirro, V. I. Tretyak, Nucl. Instrum. Meth. A 613 (2010) 54-57.

[30] U. Kolitsch, Z. Kristallogr. 216 (2001) 449-454.

[31] D. Mikhailova, N. N. Bramnik, K. G. Bramnik, P. Reichel, S. Oswald, A. Senyshyn, D. M. Trots, H. Ehrenberg, Chem. Mater. 23 (2011) 3429-3441.

[32] G. Blasse, Z. Anorg. Allg. Chem. 331 (1964) 44-50.

[33] D. E. Cox, R. J. Cava, D. B. McWhan, D. W. Murphy, J. Phys. Chem. Solids 43 (1982) 657-666.

[34] K.-H Lii, R.E.McCarley, S. Kim, R.A. Jacobson, J. Solid State Chem. 64 (1986) 347-358.

[35] N. N. Ledentsov, V. A. Shchukin, M. Grundmann, N. Kirstaedter, J. Böhrer, O. Schmidt, D. Bimberg , V. M. Ustinov, A. Yu. Egorov, A. E. Zhukov, P. S. Kop'ev, S. V. Zaitsev, N. Yu. Gordeev, Zh. I. Alferov, A. I. Borovkov, A. O. Kosogov, S. S. Ruvimov, P. Werner, U. Gösele, J. Heydenreich, Phys. Rev. B 54 (1996) 8743-8750.

[36] J. A. Groenink, C. Hakfoort, G. Blasse, phys. stat. sol. (a) 54 (1979) 329-336.